High Temperature Corrosion of Materials (2024) 101:331–350
https://doi.org/10.1007/s11085-024-10224-3

ORIGINAL PAPER

High Temperature Corrosion in Water Vapor of Fe–2.25Cr–0.54Mo Coated with Ni-Based Alloy Containing WC–Co Using an HVOF Spraying Technique

Jennarong Tungtrongpairoj[1] · Penpisuth Thongyoug[1] · Thanasak Nilsonthi[1] · Somrerk Chandra-ambhorn[1]

Received: 1 November 2023 / Revised: 2 January 2024 / Accepted: 12 January 2024 /
Published online: 9 February 2024

Abstract

The high temperature corrosion of Fe-2.25Cr-0.54Mo steel coated with WC–Co/NiCrFeSiB using a high-velocity oxy-fuel spraying technique was investigated. Coated and uncoated steel samples were tested in air and in a humidified atmosphere consisting of N_2-50%, O_2-10%, and H_2O at 750 °C for 120 h. Microstructural and phase analyses of the studied samples were performed by scanning electron microscopy equipped with energy-dispersive spectroscopy and X-ray diffraction. When compared to oxidation in air, the oxidation rate of the uncoated sample in the humidified atmosphere was faster. This occurred because there was a thicker and denser iron oxide layer at the outer subscale, and the thicker layer of inner iron oxide subscale contained chromium (Cr). Moreover, the WC–Co/NiCrFeSiB coating greatly suppressed the rates of oxidation in both the air and the humidified oxygen atmospheres. This occurred because the formation of magnetite (Fe_3O_4) was suppressed, while the protective oxides, especially nickel–chromium (Ni–Cr) spinel and chromia (Cr_2O_3) were formed during oxidation. Water vapor in the atmosphere enhanced the oxidation rate of the coated steel, with higher iron-containing oxide forming as a subscale at the outer coating.

✉ Somrerk Chandra-ambhorn
somrerk.c@eng.kmutnb.ac.th

[1] High Temperature Corrosion Research Centre, Department of Materials and Production Technology Engineering, Faculty of Engineering, King Mongkut's University of Technology North Bangkok, 1518, Pracharat 1 Road, Wongsawang, Bangsue, Bangkok 10800, Thailand

Graphic Abstract

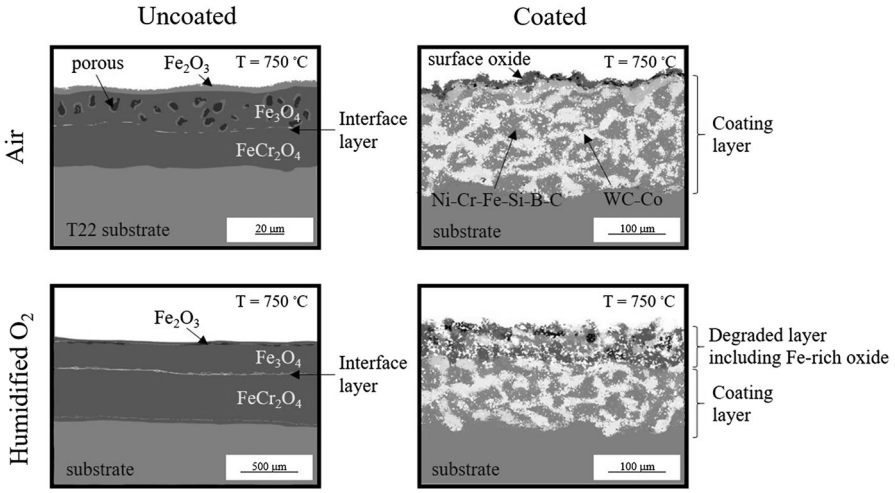

Keywords High temperature corrosion · Water vapor · Fe–2.25Cr–0.54Mo · HVOF

Introduction

Fe–2.25Cr–0.54Mo is a low alloy steel that is widely used in many high temperature applications such as in power plants [1–3]. Durability of the material is of vital importance since failure of the steel structure can result in loss of life or plant shutdown, leading to reduced economic operation. Material durability strongly depends on the operating conditions, particularly the gas composition or the deposits. Water vapor is a gaseous atmospheric component [4, 5] which severely increases steel oxidation rates at high temperatures [6–8]. The presence of water vapor in the atmosphere increases the alloy oxidation rate [9] and leads to structural failure. In boiler tube materials, non-protective oxide scales composed of an outer iron oxide layer (Fe_2O_3 and Fe_3O_4), a middle Fe–Cr oxide layer and Cr-rich oxides formed more rapidly in water vapor condition than protective chromia scales in a high percentage oxygen environment [10]. The degradation of bare steel can be mitigated by an appropriate coating. The high-velocity oxy-fuel (HVOF) spraying technique is an effective method that produces a relatively thick coating with good adherence to the steel substrate [11–13]. Appropriate powder selection improves the properties of the coating, with Ni–Cr alloy powder increasing high temperature oxidation and hot corrosion resistance, while WC powder increases wear resistance [14]. Cermet-type coatings containing different powders have been designed to combine the beneficial effects of each powder type. Mixed powders have been extensively studied including WC–Co [15–19], Cr_2C_3-NiCr [14, 20, 21], Cr_2C_3-WC-NiCr [22], and NiCr [23].

The effect of water vapor on high temperature corrosion of coated steels such as iron [24–26], low carbon steel [27], low alloy steel [24, 28], and HVOF-sprayed coated steels [13, 29, 30] is still not well understood. Bertrand et al. [24] conducted an experiment to determine the dominant defects responsible for the growth of each subscale formed on iron exposed to water vapor. A schematic sketch of the oxidation mechanism of low alloy steel in water vapor has also been presented [28, 31, 32]. However, a comprehensive explanation using a set of defect reactions to describe the scale formation phenomenon remains elusive. Volatilization of the protective oxide on the steel grade by water vapor contributing to accelerated oxidation was also considered [28], but a thermodynamic assessment of metal loss from this process has not been documented. The HVOF spraying technique is used to produce a thermal barrier coating (TBC) layer that promotes the properties of equipment installed in a high temperature environment [33], with NiCr-base alloy recommended as a coating to combat high temperature oxidation in dry and wet oxygen atmospheres [34, 35]. Several studies reported that 5–25Cr alloys formed chromia scales that exhibited a higher growth rate in wet than dry atmospheres [34, 36]. Due to the high growth rate of chromia scales in wet gases, the oxidation rate decreased [37]. By contrast, when NiCr-base alloys were oxidized the oxide layers consisted of an internal oxidation zone, inner oxide layer, and outer oxide layer with numerous voids [34]. These porous oxide layers promoted coating spallation, while the low mixed-oxide growth rate in thermally grown oxide (TGO) with a uniform and dense protective oxide layer decreased crack propagation [38].

This study investigated high temperature oxidation of T22 steel, a standard steel grade for boiler tubes [4], coated with Ni-based alloy containing WC–Co in an atmosphere containing water vapor using the HVOF spraying technique. In addition, WC–Co/NiCr alloy was generally coated for application aiming to increase the high temperature oxidation and erosion resistance [39]. This work aimed to study the HVOF-coated WC–Co/NiCrFeSiB alloys on T22 for high temperature oxidation and corrosion occurring in a simulated humidified atmosphere at 750 °C above a superheater steam temperature (about 565 °C) [4] in coal fire power plants. Defect reactions of the oxide scale growth during the oxidation process and a thermodynamic assessment of the volatilization effect were also investigated.

Experimental Procedures

Material and Coating Preparation

Ferritic steel (SA213-T22) specimens $10 \times 15 \times 5$ mm^3 were used, with their chemical compositions shown in Table 1. All specimens were polished using 600-grit SiC abrasive paper and cleaned with acetone. Some specimens were spray coated with WC–Co/

Table 1 Chemical composition of SA213-T22 (wt%) (Spectrolab Model: M8)

C	Si	Mn	S	P	Cr	Mo	Ni	Fe
0.139	0.274	0.469	0.008	0.014	2.040	0.976	0.035	bal

NiCrFeSiB alloy powder containing 88%WC–12%Co particles and NiCrFeSiB alloy particles at a 50:50 ratio by weight. These powder mixtures were magnified by SEM, as shown in Fig. 1. The chemical composition from the producer was 44WC–6Co–36Ni –8Cr–2Fe–2Si–1.7B–0.3C wt%.

The T22 specimens were sprayed using a JP-5000 HVOF thermal spray system with coating details reported by [40] as kerosene 5.2 gph*, O_2/fuel ratio 385 scfh**/gph, spray distance 390 mm, powder feed 120 g min^{-1}, and carrier gas 23 L min^{-1} (*gph = gallons per hour, **scfh = standard cubic feet per hour).

High Temperature Oxidation Test and Material Characterization

Coated and uncoated specimens were tested in air and in a humidified atmosphere (N_2-50%O_2-10%H_2O) in a quartz tube furnace at 750 °C. Water vapor in the humidified atmosphere was produced by boiling deionized water (DI water) at 44.5 $^{\circ}$C, giving water vapor partial pressure of 0.1 bar, calculated using standard thermodynamic data [41]. High temperature exposure times were 24, 48, 72, 96, and 120 h.

Following high temperature exposure, the samples were cooled to room temperature by argon. Sample weights were measured before and after exposure using a five-digit balance. An X-ray diffractometer (D8 Bruker) was used to identify the phases formed using the standard XRD patterns compiled by the International Centre for Diffraction Data (ICDD). The incident Cu-Kα line, $\lambda = 1.5406$ Å, at 40 kV and 40 mA was utilized in XRD analysis with scanning speed 0.05 °/sec, range angle $2\theta = 15–85°$, and sampling width 0.02°. Bare specimens after the oxidation test were polished to identify phases on the outer and inner oxide layers by XRD. The cross-sectional morphology and element intensities of the coating and the oxide were analyzed by a scanning electron microscopy (SEM) equipped with energy-dispersive spectroscopy (EDS). The oxide scale thickness on the specimens was measured at five different locations. The mode of high-resolution images of shapes of objects (SEI) with EDS analysis was used at 15 keV depending on the microscopic resolution of each specimen. Void sizes in the scale layers on both bare and coated specimens after oxidation were measured using the ImageJ program to compare the

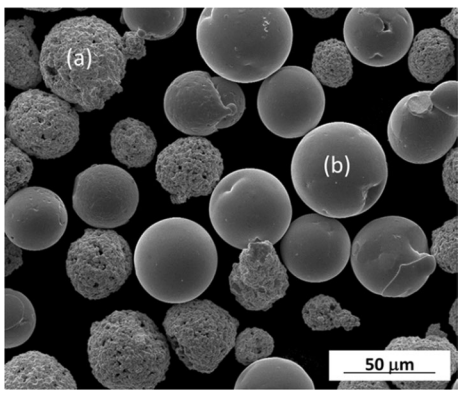

Fig. 1 SEM morphology of the mixed powders showing a 88%WC–12%Co (50 wt%) particles size 87.28 µm, and **b** Ni–Cr–Fe–Si–B–C (50 wt%) particles size 42.32 µm

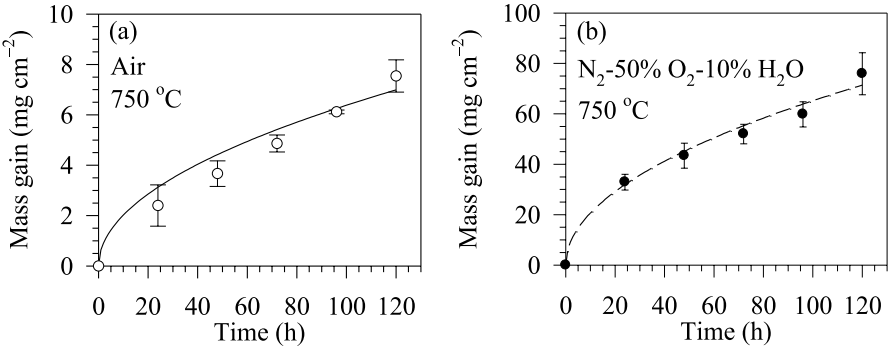

Fig. 2 Mass gain of uncoated T22 after oxidation at 750 °C in **a** air, and **b** N_2-50% O_2-10% H_2O

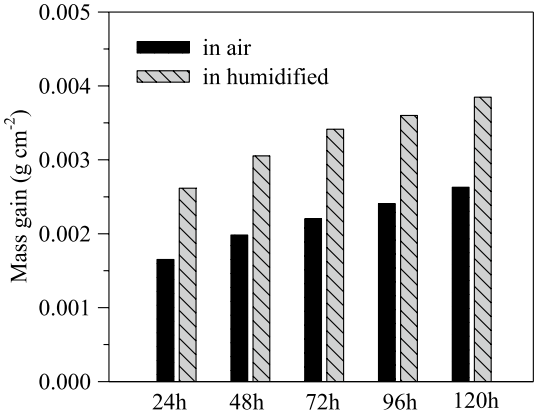

Fig. 3 Mass gains of coated T22 after oxidation in different atmospheres and time periods

cross-sectional morphology with thickness following air void analysis (ASTM C 457).

Results

Mass gain of uncoated T22 was measured after the oxidation test in air and a humidified atmosphere at 750 °C for 120 h and plotted as a function of time, as shown in Fig. 2. Mass gain of the uncoated sample oxidized in air was lower than in humidified oxygen as 7.5 mg cm^{-2} and 75.9 mg cm^{-2}, respectively. However, the spallation of scale layer (the debris spalled out from the samples collected in a crucible) occurred on the coated sample after the oxidation test under both conditions. Mass gain of the coated sample was only from the scale remaining on the sample after the oxidation test as shown in a bar chart (Fig. 3). The spallation of the coated sample was relatively significant after exposure for 24 h. The mass of coating spallation (the mass of the collected spalled scales normalized by the sample surface) in both

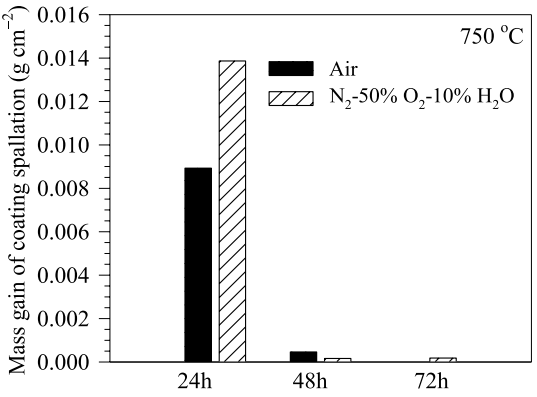

Fig. 4 Mass of coating spallation of coated T22 after oxidation in different atmospheres and time periods

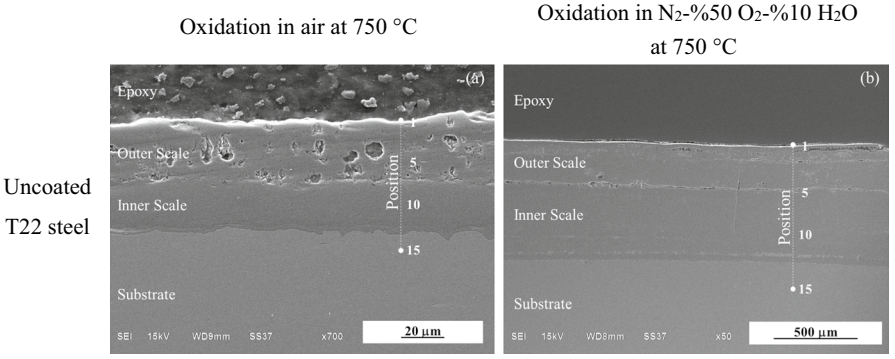

Fig. 5 SEM cross-sectional images of **a** uncoated sample in air, and **b** uncoated sample in N_2-50% O_2-10% H_2O after oxidation at 750 °C for 120 h

atmospheres reduced at longer oxidation periods, with the mass of coating spallation in a humidified atmosphere greater than in air (Fig. 4).

Uncoated T22 Steels

Cross sections of the uncoated samples after exposure in air and humidified oxygen at 750 °C for 120 h are shown in Fig. 5. The scale of the uncoated sample oxidized in air was 52 ± 2 µm thick (Fig. 5a) with two main outer and inner subscales. The outer subscale consisted of embedded voids and was 30 ± 2 µm thick, while the inner denser subscale was 23 ± 1 µm thick. The scale of the uncoated sample oxidized in a humidified atmosphere was thicker than the former by 15 µm and consisted of two main subscales separated by an explicit internal crack line (Fig. 5b). There were several large voids 5 ± 2 µm in size in the outer subscale of the oxidized sample in air, as shown in Fig. 6 but only a few voids in the outer subscale of the oxidized sample in a humidified atmosphere. Notably, there were numerous voids and pores with different sizes in the scale of the uncoated sample oxidized in air, leading to large

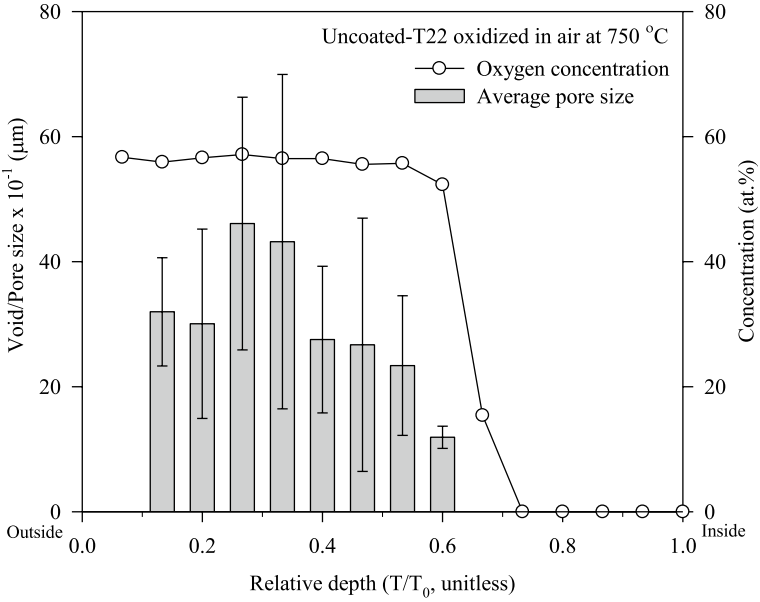

Fig. 6 Oxygen concentration and void and pore sizes of uncoated T22 scale oxidized in air at 750 °C for 120 h. (*Note*: T = scale thickness and T_0 = total scale thickness of the outer subscale)

deviations in void and pore size, as illustrated in the bar chart. EDS results of both samples showed the Fe and O peaks in both subscales, with an additional amount of Cr in the inner subscale, as shown in Table 2. High atomic percentage of oxygen was detected in the outer subscale with high atomic ratio of Fe and O at 0.5–0.7 as the hematite (Fe_2O_3) structure. The XRD pattern (Fig. 7) confirmed the existence of Fe_2O_3 in the outer subscale layer and in both layers after oxidation in a humidified and air atmosphere, respectively. Moreover, the peak of chromite ($FeCr_2O_4$) was only present in the inner layer for both testing conditions.

Coated T22 Steels

The cross section of coated T22 before the oxidation test was revealed by SEM–EDS as a compact lamellar structure (Fig. 8). The compact coating layer thickness was 451 ± 17 μm and consisted of two different phases as WC–Co–Ni–Fe phase (light area) and Ni–Cr–C–Fe-Si–W phase (dark area). Globular voids appeared at the outer subscale and the coating/substrate internal interface at 2.2 ± 1 μm, as depicted in the higher magnification SEM image [Fig. 8 (right-hand side)]. After oxidation in both atmospheres, coating thickness decreased, as shown in Fig. 9 and Fig. 10, and the outer subscale coating deteriorated, particularly for the sample oxidized in a humidified atmosphere. Figure 9b, c shows larger voids compared to the voids in the as-coated layer at the outermost, middle, and interface of the coating. An internal crack was visible between

Table 2 Normalized element intensities (Fe and Cr) of the uncoated sample oxidized in a humidified atmosphere and measured using a cross-sectioned sample (Fig. 5b)

Position	Depth (μm)	Normalized atomic ratio*		Presence of O
		Fe	Cr	
1	0	1.000	0.000	✓
2	72.4	0.985	0.015	✓
3	144.8	0.991	0.009	✓
4 (i/f)	217.2	0.983	0.017	✓
5	289.6	0.958	0.042	✓
6	362	0.968	0.032	✓
7	434.4	0.962	0.029	✓
8	506.8	0.958	0.038	✓
9	579.2	0.954	0.040	✓
10	651.6	0.971	0.028	✓
11	724	0.949	0.046	✓
12	796.4	0.975	0.025	–
13	868.8	0.976	0.024	–
14	941.2	0.976	0.024	–
15	1013.6	0.976	0.024	–

*A normalized atomic ratio is defined as the atomic percentage of the interested element per atomic percentage of Fe, Cr, and Mn

the outer and inner coating layers after oxidizing in a humidified atmosphere. The void percentage in the coating layer was high at 10.1% after oxidation in a humidified atmosphere, and more than ten times higher than after oxidizing in air and as-coating. The void percentage in the as-coating layer was not more than 2%, as the normal porosity range after HVOF thermal spray coating [42] and slightly increased after oxidizing in air, as shown in Fig. 11.

Six EDS analyses were carried out from points 1 to 6, as shown in Figs. 9 and 10. The atomic ratios of Fe per atomic ratios of cations (Fe, Cr, Co, Ni, W, and Si) of the coated samples oxidized in both atmospheres are listed in Table 3. The high atomic percentage of Fe at points 1 and 2 indicated the iron interstitial for iron oxide formation, which corresponded to the deterioration area of the sample oxidized in a humidified atmosphere, while this phenomenon was not observed in the sample oxidized in air. The EDS results showed a good agreement with the XRD results (Fig. 12), with only Fe_2O_3 (ICDD 02-0919) was detected in the scale oxidized in a humidified atmosphere. Thus, it can be concluded that the Fe_2O_3 presented in the outer coating layer after oxidizing in a humidified atmosphere. The peaks of WC (ICDD 89-2727) and CrNi (ICDD 65-5559) were observed in the as-coated sample, while major peaks of Ni-Cr spinel (ICDD 89-4630) and minor peaks of $NiWO_4$ (ICDD 72-0480), Cr_2O_3 (ICDD 82-1484), Fe_3C (ICDD 76-1877), and WC (ICDD 89-2727) were presented after oxidation in both conditions. The Ni–Cr spinel and $NiWO_4$ were determined as detrimental mixed oxides by Savisha Mahalingam et al. [38] causing disastrous horizontal and compressive cracks in the scale, thereby deteriorating the coating layer, as discussed in the next section.

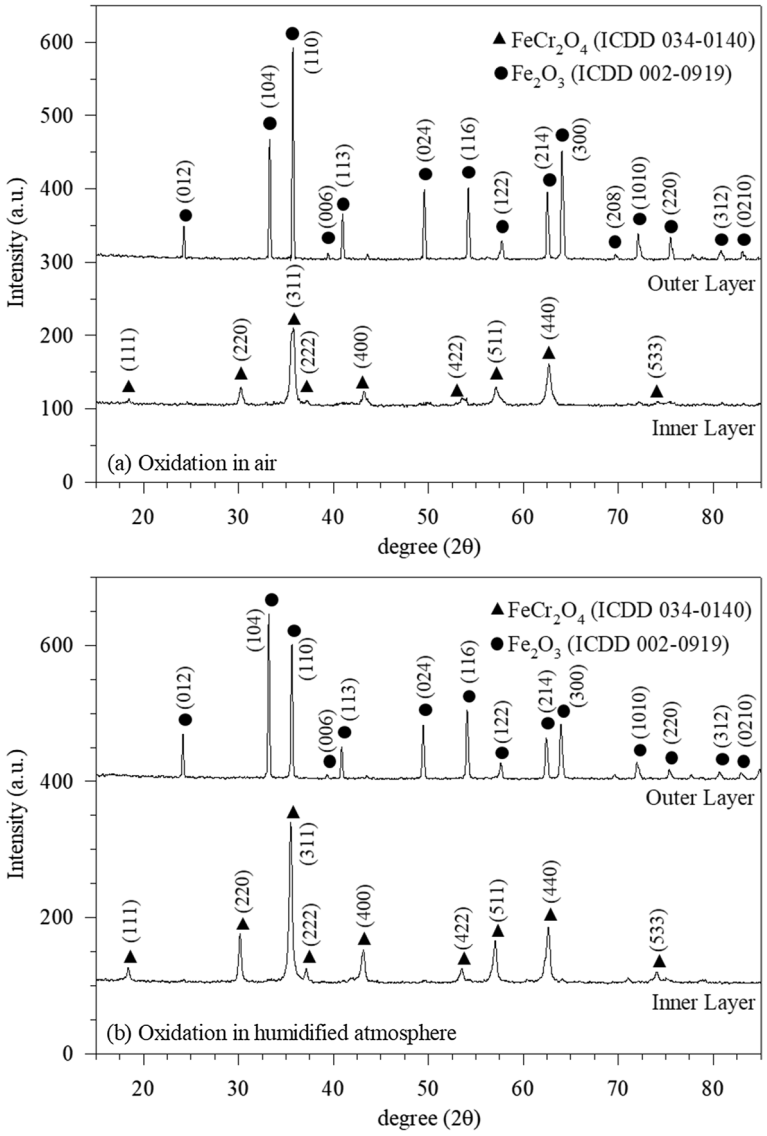

Fig. 7 XRD patterns of uncoated T22 oxidized at 750 °C for 120 h in **a** air, and **b** a humidified atmosphere

Discussion

Mass gains of uncoated and coated T22 were determined by parabolic oxidation kinetics, with results indicating that oxide growth was diffusion-controlled. Figure 13 presents the parabolic rate constants of the studied samples in an Arrhenius form together with data from the literature [3, 14, 43–49]. The rate constants of the

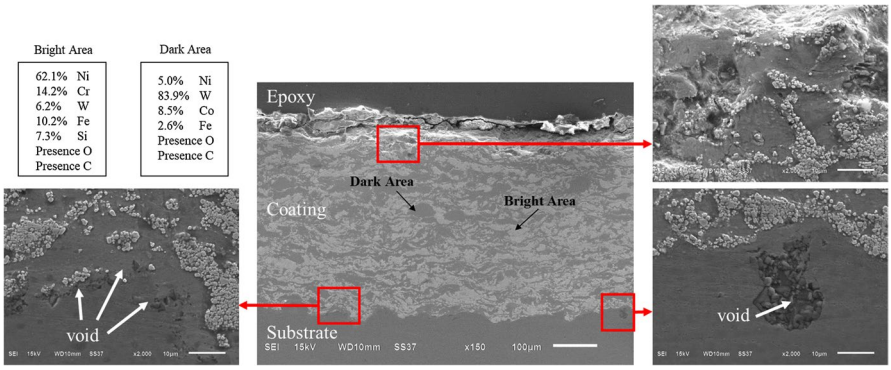

Fig. 8 SEM cross-sectional images of coated T22 before oxidation

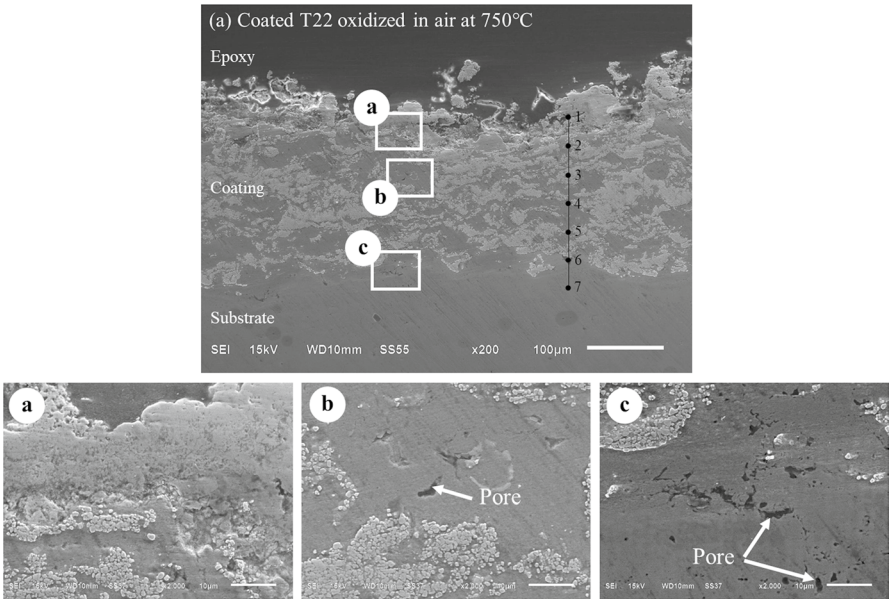

Depth (μm)	Position	at.%						
		Ni	Cr	W	Co	Fe	Si	O
37	1	20.82	4.00	50.84	18.05	6.29	-	✓
74	2	31.47	57.55	1.88	4.42	3.37	1.32	-
111	3	51.29	26.08	3.86	6.44	5.82	6.51	✓
148	4	74.13	5.29	1.18	7.97	11.44	-	✓
185	5	59.67	14.38	5.52	6.35	6.93	7.15	✓
222	6	-	-	-	-	100.00	-	✓
259	7	-	1.48	-	-	98.52	-	-

Fig. 9 SEM cross-sectional images of the coated sample in air after oxidation at 750 °C for 120 h (Remark: = ✓ the presence of oxygen)

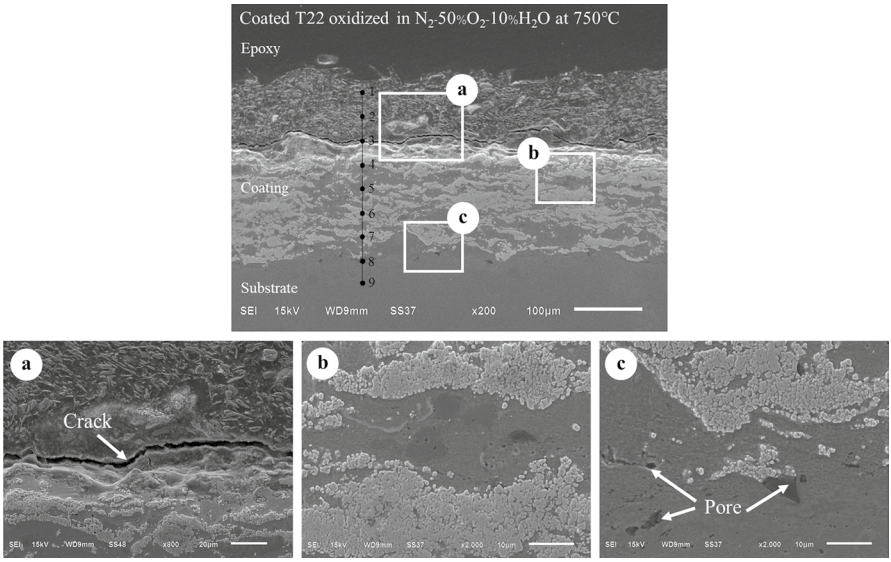

Depth (μm)	Position	at.%						
		Ni	Cr	W	Co	Fe	Si	O
36	1	-	3.06	-	-	96.94	-	✓
72	2	1.57	2.48	-	-	95.95	-	✓
108	3	22.21	-	8.15	-	69.64	-	✓
144	4	31.93	21.48	34.44	5.22	3.40	3.53	✓
180	5	54.17	26.20	-	9.91	4.62	5.09	✓
216	6	-	-	89.59	2.52	7.90	-	-
252	7	50.62	13.13	2.97	-	27.28	6.01	-
288	8	-	1.84	-	-	98.16	-	-
324	9	-	8.23	-	-	91.77	-	-

Fig. 10 SEM cross-sectional images of the coated sample in N_2-50% O_2-10% H_2O after oxidation at 750 °C for 120 h (Remark: = ✓the presence of oxygen)

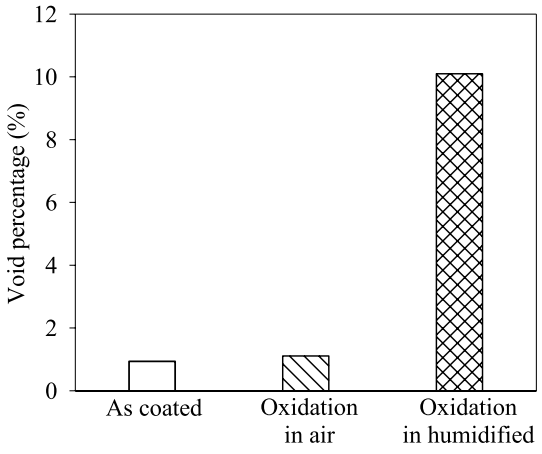

Fig. 11 Void percentages of the coating layers oxidized in air and a humidified atmosphere at 750 °C for 120 h

Table 3 Atomic ratios of Fe per total atomic ratios of cations (Fe, Cr, Co, Ni, W, and Si) of coated samples oxidized in air and a humidified atmosphere (Figs. 9 and 10)

Position	Normalized atomic ratio of Fe		Presence of O	
	Air	N_2-50% O_2-10% H_2O	Air	N_2-50% O_2-10% H_2O
1	0.06	0.97	✓	✓
2	0.03	0.96	–	✓
3	0.06	0.70	✓	✓
4	0.11	0.03	✓	✓
5	0.07	0.05	✓	✓
6	1.0	0.08	✓	–
7	0.99	0.27	–	–
8	–	0.98	–	–
9	–	0.92	–	–

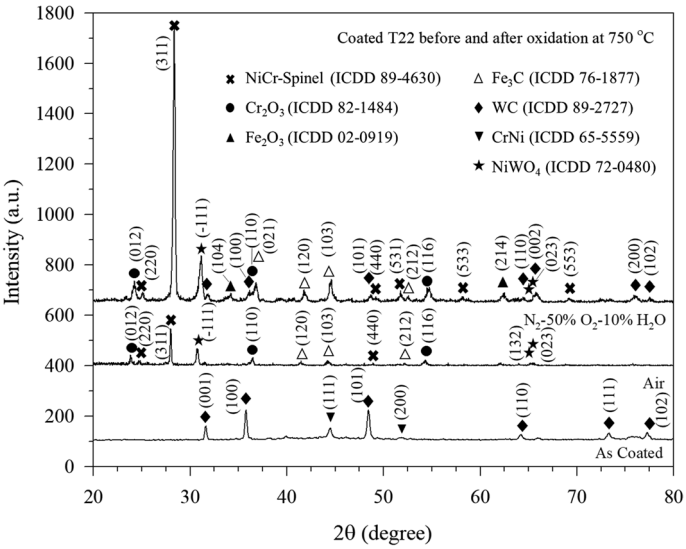

Fig. 12 XRD patterns of coated T22 before and after oxidation at 750 °C for 120 h in air and N_2-50% O_2-10% H_2O

uncoated steel were lower than for T22 reported in the literature and above the rate constants for the formation of chromia on stainless steels. The lower rate constant of uncoated T22 was observed by Singh et al. [14] at a lower temperature of 700 °C, as listed in Table 4. Likewise, the very low-rate constants were reported in the research studies carried out on high chromium and nickel substrates such as SS304 and Ni-5Cr [34, 39]. This occurred possibly due to the chromia formation and excellent corrosion resistance properties of nickel when compared to the studied steel substrate in this work.

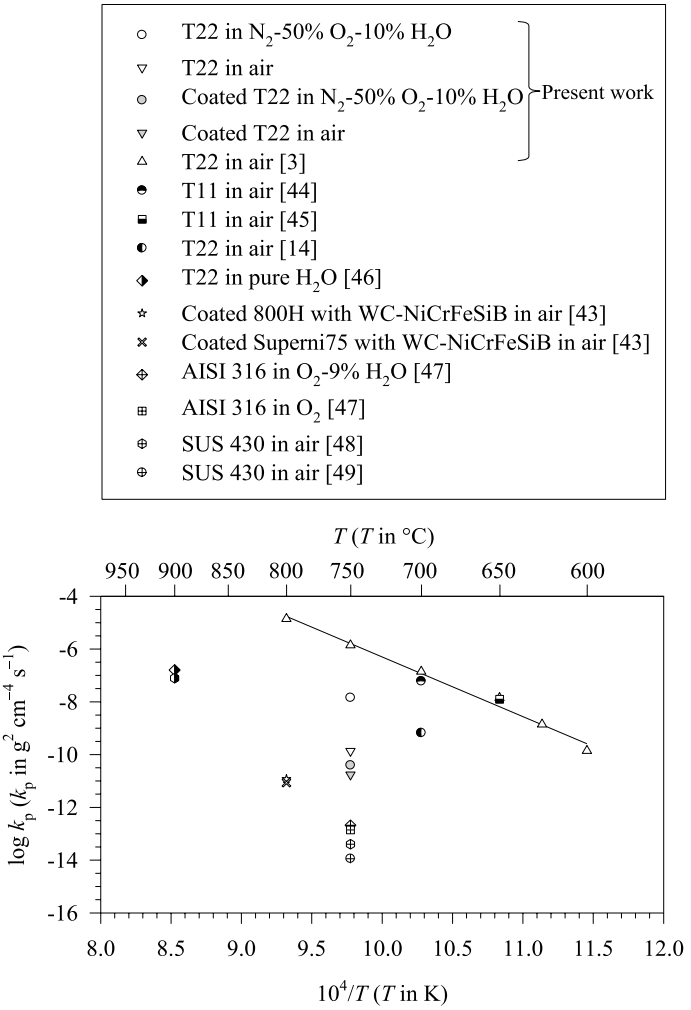

Fig. 13 Arrhenius plots of the parabolic rate constants for oxidation of the studied steels and those from other literature [3, 14, 43–49]

The rate constants of uncoated and coated steel oxidized in water vapor were significantly higher than for oxidation in air. When the uncoated steel was oxidized in the humidified atmosphere, the oxidation rate was enhanced. The outer subscale was also nearly free from voids, while they were significantly observed in the scale formed in the air. This part of the scale thickened from 52 µm for the uncoated sample oxidized in air to 78 µm for the uncoated sample oxidized in the humidified atmosphere. Having the same trend, the inner subscale also drastically increased, i.e., from 23 µm for the uncoated sample oxidized in air to 47 µm for the uncoated sample oxidized in the humidified atmosphere. The accelerated oxidation rate should be from the more rapid oxygen diffusion through the oxide scale, which can be the molecular or ionic diffusion

Table 4 Calculated parabolic rate constants (k_p) in different environments at 750 °C

Description and environment	k_p (10^{-5} mg^2 cm^{-4} s^{-1})
(Uncoated T22: This study)	
in air	10.95
in 10%H_2O containing	1180.56
(WCCo-NiCrFeSiBC coated on T22: This study)	
in air	8.33
in 10%H_2O containing	16.67
Uncoated T22 in air at 700 °C [14]	1.56
(Uncoated Ni-5Cr at 650 °C)	
in Ar-20%O_2-20%H_2O [34]	0.13
in Ar-20%H_2O [34]	0.003
(NiCrSiB/WCCo coated on SS304)	
in air [39]	0.04

of oxygen-containing species. The acceleration can promote the oxide thickness and density, concurred with the mechanism of the rapid growth rate of wustite thermally grown on iron oxidized in water vapor by the void movement due to molecular water vapor proposed by Rahmel and Tobolski [26]. The growth of the outer subscale relating to its thickness and density reasonably results from the inward oxygen diffusion to form hematite at the scale/gas interface, while the growth of the inner subscale was mainly from the cation vacancy diffusion to form $FeCr_2O_4$ spinel [50] followed by the XRD results in Fig. 7.

When the steel was coated, the rate constant reduced toward chromia growth values and suppressed the oxidation rate of the steel. For example, the mass gain of the uncoated sample oxidized in air for 120 h was 7.1×10^{-3} g cm^{-2}. The coating reduced the mass gain by about 2.7 times to 2.6×10^{-3} g cm^{-2} after oxidation for the same period. For the oxidation in a humidified atmosphere, the mass gain of the uncoated sample after 120 h exposure was 84×10^{-3} g/cm^2. The coating reduced the mass gain to a greater extent, i.e., by about 22 times to 3.8×10^{-3} g cm^{-2} after oxidation for the same period. Figure 14 shows the lines presenting the equilibrium oxygen partial pressure of the formation of oxides using standard thermodynamic data [33] in a furnace in air and in N_2-50%O_2-10%H_2O plotted as a function of the reciprocal temperature. The formation mechanisms of oxides are represented in Eqs. 1–5, as shown below.

$$\frac{4}{3}\mathrm{Fe} + \mathrm{O_2} = \frac{2}{3}\mathrm{Fe_2O_3} \quad (1)$$

$$\frac{4}{3}\mathrm{Cr} + \mathrm{O_2} = \frac{2}{3}\mathrm{Cr_2O_3} \quad (2)$$

$$\mathrm{Ni} + 2\mathrm{Cr} + 2\mathrm{O_2} = \mathrm{NiCr_2O_4} \quad (3)$$

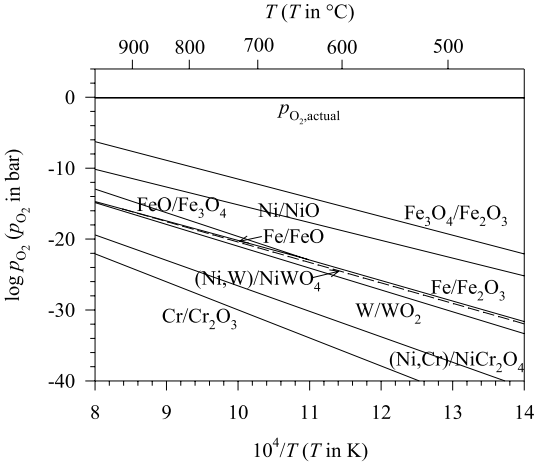

Fig. 14 Equilibrium partial pressures for the formation of oxides relevant to this study at different temperatures calculated using thermodynamic reference data [55]

$$Fe + \frac{1}{2}O_2 + Cr_2O_3 = FeCr_2O_4 \quad (4)$$

$$Ni + W + 2O_2 = NiWO_4 \quad (5)$$

The partial pressures of oxygen in both studied atmospheres were higher than those required to form Fe_2O_3, Cr_2O_3, $NiCr_2O_4$, and $NiWO_4$. This analysis indicated the thermodynamic stability at the standard state of the oxides formed in the studied atmospheres, i.e., Fe_2O_3 and Fe_3O_4 for the uncoated samples, and $NiCr_2O_4$, Cr_2O_3, $NiWO_4$ and Fe_2O_3 for the coated samples, as analyzed by XRD.

When HVOF thermal spraying was applied on the uncoated sample, WC–Co coatings were obtained, as shown in Fig. 8. A compact coating layer of two phases as rich W–C and Ni–Cr was formed and confirmed as WC and CrNi by XRD analysis. The formation of these two phases was also observed after HVOF spraying of the WC–Co powders mixed with NiCr–Cr_3C_2 powders on the same steel grade, as reported by Singh et al. [12]. When the coated steel was oxidized in air and humidified atmospheres, oxidation considerably reduced. Formation of $NiCr_2O_4$ and Cr_2O_3 contributed to this beneficial effect as protective oxides. It is well known that formation of Cr_2O_3 helps to protect steel from high temperature corrosion of Cr-containing steel [44–48]. When the coated steel was oxidized in a humidified atmosphere, the oxidation rate was lower than the uncoated sample but oxidized faster and suffered from spallation more than in air. This behavior related to the formation of non-protective iron-rich oxide, i.e., hematite in the coating layer after oxidation in a humidified atmosphere, as shown in Fig. 10. Hematite in the scale was formed by inward diffusion of oxygen, where the iron site (Fe) reacted with oxygen in the atmosphere, according to Eq. 6. This formation was also observed by F. Liu et al. who developed a non-protective thick scale on X20 stainless steel samples after exposure in O_2 containing 40%H_2O at 600 °C for 336 h [51]. However, the formation of magnetite (Fe_3O_4) grown by the cation vacancy [24]

was suppressed probably due to the formation of $NiCr_2O_4$ spinel from the relatively high diffusion coefficient of cation through NiO (non-stoichiometric NiO), as reported by Chatterjee et al. [11]. The formation of the Ni–Cr spinel as well as Cr_2O_3, primarily resulting from high chromium content in the inner subscale, also helped to protect the studied steel against corrosion. Thus, the protective oxides at the inner subscale can provide corrosion resistance for steel substrates to prevent oxidation in air and humidified atmospheres.

$$2\underline{Fe} + \frac{3}{2}O_2 \rightarrow 2(Fe_{Fe})_h + 3(O_O)_h \tag{6}$$

where the subscripts h and o indicate that the interested entity is in the hematite as the outer scale layer.

As well as hematite formation, the detrimental mixed oxides of thermally grown oxides (TGOs) such as $NiCr_2O_4$, Cr_2O_3, and $NiWO_4$ also promoted cracks and led to spallation. Our results concurred with Savisha Mahalingam et al. who found that microcracks were caused by mixed clusters of $((Cr,Al)_2O_3)$, spinel $(Ni(Cr,Al)_2O_4)$, and nickel oxide (NiO), while the many pores at the coating/substrate interface induced compressive stresses, and hence, horizontal and compressive cracks. Mixed oxides caused high stress in the surrounding area that initialized the cracking formation [38, 52, 53].

The high severity of the deterioration of the coating layer after exposure in a humidified atmosphere can be explained by the oxidation and chromia volatilization in water vapor. Rapid oxidation of coated steel oxidized in humidified oxygen results from the ionic transport of oxygen. Water vapor is incorporated into the oxide in a hydroxyl OH^- form. When hydrogen bonds with oxygen to form hydroxyl ions, the ionic radius is reduced from 140 to 95 pm for OH^- [43]. As a result, the hydroxyl species can rapidly diffuse through the oxide or along the grain boundaries to the inner subscale and accelerate oxidation in the subscale. Formation of $NiCr_2O_4$ and $NiWO_4$ was detected after exposure of the coated steel in a humidified atmosphere. It is then possible that the volatilization of the Ni–Cr spinel, giving Cr-containing volatile species and $NiWO_4$, may also occur according to Eqs. 7–9.

$$\frac{1}{2}Cr_2O_3 + \frac{3}{4}O_2 + H_2O \rightarrow CrO_2(OH)_2 \tag{7}$$

$$\frac{1}{2}NiCr_2O_4 + \frac{3}{4}O_2 + H_2O \rightarrow CrO_2(OH)_2 + \frac{1}{2}NiO \tag{8}$$

$$\frac{1}{2}NiCr_2O_4 + \frac{3}{2}O_2 + \frac{1}{2}W + H_2O = CrO_2(OH)_2 + \frac{1}{2}NiWO_4 \tag{9}$$

Another volatile phase that can occur in dry oxygen is CrO_3 [49], shown in Eq. 10. The Ni–Cr spinel may also be volatilized giving CrO_3 by Eqs. 11 and 12.

$$\frac{1}{2}Cr_2O_3 + \frac{3}{4}O_2 \rightarrow CrO_3 \tag{10}$$

$$\frac{1}{2}NiCr_2O_4 + \frac{3}{4}O_2 \rightarrow CrO_3 + \frac{1}{2}NiO \tag{11}$$

$$\frac{1}{2}NiCr_2O_4 + \frac{3}{2}O_2 + \frac{1}{2}\mathrm{W} = CrO_3 + \frac{1}{2}NiWO_4 \tag{12}$$

Partial pressures of the $CrO_2(OH)_2$ volatile species were calculated using thermodynamic data from Opila et al. [54] and Kubaschewski et al. [55], with results presented in Fig. 15. At 700 °C, partial pressures of the $CrO_2(OH)_2$ volatile species were 8.08×10^{-7} and 3.98×10^{-7} bar for the volatilisation in a humidified atmosphere, following Eqs. 7 and 8, respectively. At the same temperature, partial pressures of the CrO_3 volatile species from volatilization in air according to Eqs. 10 and 11 were 8.84×10^{-10} and 4.41×10^{-10} bar, respectively. For both volatilizations from Cr_2O_3 and $NiCr_2O_4$, the partial pressure of the volatile Cr-species formed in a humidified atmosphere ($CrO_2(OH)_2$) was enhanced by about 1000 times that formed in oxygen (CrO_3). This contributed to void generation following the mechanism of Rahmel Tobolski mechanism [26] and formation of iron oxide to a greater extent in the outer subscale coating, as confirmed by the EDS result in Fig. 10. This supported Fe_2O_3 formation in the outer coating layer and the existence of microcracks at the outer/inner coating interface, resulting in more severe deterioration of the coating, as seen in Fig. 10. It is noteworthy that the volatilizations of Cr_2O_3 and Ni–Cr spinel in a humidified atmosphere are a specific interaction which can accelerate the Cr diffusion and enhance oxidation in coating layers and could potentially lead to the breakaway oxidation as presented in a previous study on oxidation and volatilization damage behavior of NiCr coatings in air-H_2O environment at 650 °C [56].

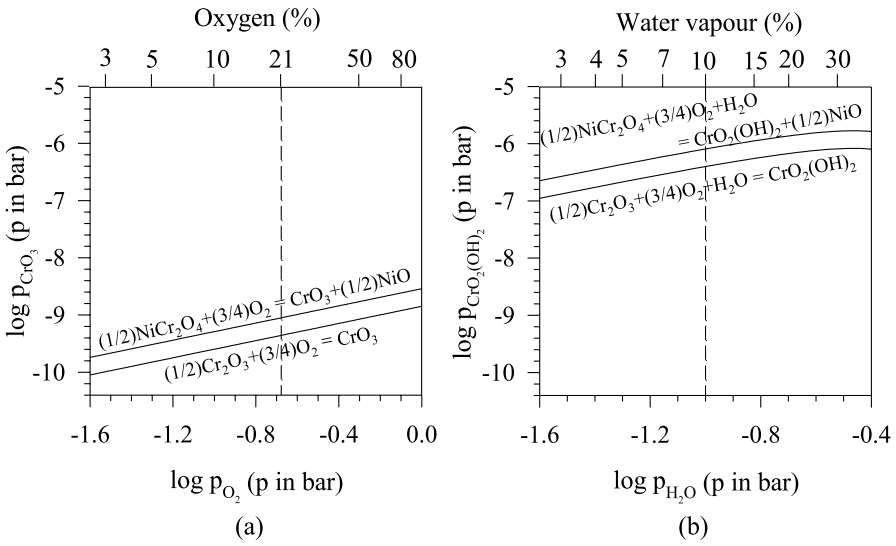

Fig. 15 Equilibrium partial pressures of volatile Cr-species formed in **a** air, and **b** N_2-50% O_2-10% H_2O, calculated using thermodynamic data from Refs. [33, 55]

Conclusions

High temperature oxidation of T22 in air and humidified atmospheres reduced after applying Ni-based HVOF thermal spray coating. The humidified atmosphere of N_2-50% O_2-10% H_2O resulted in an aggressive oxidation and promoted high oxidation rate on both uncoated and coated steels. The oxide scale consisted of a highly porous Fe_2O_3 outer layer and an inner $FeCr_2O_4$ layer after oxidizing in air, with denser and thicker scale after oxidizing in a humified atmosphere. Deterioration of the coated steel occurred due to the oxidation dominated by the inward diffusion of oxidants from the water vapor and chromia volatilization, with the deterioration mechanism summarized as follows:

- The WC–Co/NiCrFeSiB coating layer oxidized and volatized in air and humidified atmospheres to Cr_2O_3, $NiWO_4$, and Ni–Cr spinel and spalled greatly after exposure for 24 h.
- Fe_2O_3 formed at the outer coating layer due to the high partial pressures of the volatile chromium species in a humidified atmosphere, following the thermodynamics data.
- The percentages of voids and pores were high inside the coating layer, especially at the coating/substrate internal interface, caused by molecular diffusion of oxygen-containing species and molecular water vapor.
- Fe_2O_3 formation at the outer layer, pore generation, and the detrimental mixed oxides of $NiCr_2O_4$, Cr_2O_3, and $NiWO_4$ caused microcrack propagation at the outer/inner coating interface, leading to deterioration and spallation of the coating layer.

In all, the deterioration of HVOF-sprayed WC–Co/NiCrFeSiB coatings on T22 steel in water vapor examined by high temperature oxidation test and material characterization in the present work will contribute to preventing high temperature corrosion of HVOF spray coatings on common steel grades used in superheated steam environments of coal-fired power plants and their related industries. However, the observations of the coated T22 exposed to humidified atmospheres containing a higher percentage of water vapor are limited. Therefore, future investigation should be conducted to study the effect of water vapor on the high temperature corrosion behavior of the coated T22 at different water vapor percentages and the optimization of coating parameters such as feedstock powder size and coating speeds in order to achieve high coating quality and increase corrosion resistance of coating layers.

Acknowledgements This research was funded by National Science, Research and Innovation Fund (NSRF), and King Mongkut's University of Technology North Bangkok with Contract no. KMUTNB-FF-67-A-06.

Author Contributions J.T. and P.T. wrote the main manuscript text, data collected and analyzed; P.T. prepared all figures; T.N. provided funding acquisition; and S.Ch. edited and supervision. All authors reviewed the manuscript.

Funding This research was funded by National Science, Research and Innovation Fund (NSRF), and King Mongkut's University of Technology North Bangkok with Contract no. KMUTNB-FF-67-A-06.

Declarations

Conflict of interest The authors declare no known competing financial interests or personal relationships that influenced the reported contents of this paper.

References

1. A. D. Gianfrancesco (ed.), *Materials for Ultra-Supercritical and Advanced Ultra-Supercritical Power Plants*, (Woodhead Publishing Ltd, Duxford, 2017).
2. J. E. Oakey (ed.), *Power Plant Life Management and Performance Improvement*, (Woodhead Publishing Ltd, Cornwall, 2011).
3. L. W. Pinder, K. Dawson, and G. J. Tatlock, High temperature corrosion of low alloy steels. in *Shreir's Corrosion*, eds. B. Cottis, M. Graham, R. Lindsay, et al. (Elsevier, Amsterdam, 2009), p. 558.
4. G. R. Holcomb, Steam oxidation in steam boiler and turbine environments. in *Power Plant Life Management and Performance Improvement*, ed. John E. Oakey (Woodhead Publishing Ltd, Cornwall, 2011), p. 453.
5. G. Y. Lai, *High-Temperature Corrosion and Materials Applications*, (ASM International, Materials Park, 2007).
6. S. W. Liu, W. Z. Wang, and C. J. Liu, *Case Studies in Engineering Failure Analysis* **9**, 2017 (35–39).
7. A. Movahedi-Rad, S. S. Plasseyed, and M. Attarian, *Engineering Failure Analysis* **48**, 2015 (94).
8. T. Dudziak, S. Grobauer, N. Simms, U. Krupp, and M. Lukaszewicz, *High Temperature Materials and Processes* **34**, 2015 (261).
9. S. Saunders, M. Monteiro, and F. Rizzo, *Progress in Materials Science* **53**, 2008 (775).
10. J. Yuan, X. Wu, W. Wang, S. Zhu, and F. Wang, *Materials (Basel)* **7**, 2014 (2772).
11. U. K. Chatterjee, S. K. Bose, and S. K. Roy, *Environmental Degradation of Metals*, (M. Dekker, New York, 2001).
12. V. P. Sidhu, K. Goyal, and R. Goyal, *Anti-Corrosion Methods and Materials* **64**, 2017 (499–507).
13. T. S. Sidhu, S. Prakash, and R. D. Agrawal, *Surface and Coatings Technology* **201**, 2006 (792–800).
14. H. Singh, M. Kaur, and S. Prakash, *Journal of Thermal Spray Technology* **25**, 2016 (1192–1207).
15. M. M. Verdian, *Transactions of the IMF* **96**, 2018 (206).
16. J. Liu, X. Bai, T. Chen, and C. Yuan, *Coatings* **9**, 2019 (534).
17. C.-F. Yang, W.-L. Pai, C.-M. Hsu, and C.-Y. Chen, *Sensors and Materials* **31**, 2019 (531).
18. R. Ahmed, G. Vourlias, A. Algoburi, et al., *Journal of Thermal Spray Technology* **27**, 2018 (1579).
19. A. S. Praveen, J. Sarangan, S. Suresh, and B. H. Channabasappa, *Ceramics International* **42**, 2016 (1094).
20. Y. Ding, T. Hussain, and D. G. McCartney, *Journal of Materials Science* **50**, 2015 (6808).
21. W. Zhou, K. Zhou, Y. Li, C. Deng, and K. Zeng, *Applied Surface Science* **416**, 2017 (33–44).
22. W. Zhou, K. Zhou, C. Deng, K. Zeng, and Y. Li, *Ceramics International* **43**, 2017 (9390–9400).
23. H. Gada, D. Mudgal, S. Parvez, and B. Ahmad, *Engineering Failure Analysis* **108**, 2020 104256.
24. N. Bertrand, C. Desgranges, D. Poquillon, M. C. Lafont, and D. Monceau, *Oxidation of Metals* **73**, 2010 (139).
25. C. W. Tuck, M. Odgers, and K. Sachs, *Anti-Corrosion Methods and Materials* **13**, 1966 (14).
26. A. Rahmel and J. Tobolski, *Corrosion Science* **5**, 1965 (333).
27. R. Y. Chen, *Oxidation of Metals* **59**, 2003 (433).
28. D. Jiang, H. Xu, Z. Zhu, B. Deng, and N. Zhang, *Oxidation of Metals* **87**, 2017 (189).
29. A. C. Karaoglanli, M. Oge, K. M. Doleker, and M. Hotamis, *Surface and Coatings Technology.* **318**, 2017 (299).
30. J. Singh, H. Vasudev, and S. Singh, *Materials Today: Proceedings* **26**, 2020 (972).
31. T. Dudziak, M. Łukaszewicz, N. Simms, and J. Nicholls, *Oxidation of Metals* **85**, 2016 (171–187).
32. J. Bischoff and A. T. Motta, *Journal of Nuclear Materials* **424**, 2012 (261).
33. N. Bala, H. Singh, and S. Prakash, *Surface and Coatings Technology* **318**, 2017 (50).
34. C. Jiang, Y. Xie, C. Kong, J. Zhang, and D. J. Young, *Corrosion Science* **174**, 2020 108801.
35. M. Michalik, M. Hänsel, J. Zurek, L. Singheiser, and W. J. Quadakkers, *Materials at High Temperatures* **22**, 2005 (213–221).

36. J. Zurek, D. J. Young, E. Essuman, et al., *Materials Science and Engineering: A* **477**, 2008 (259).
37. M. Hänsel, E. Turan, V. Shemet, et al., *Materials at High Temperatures* **32**, 2015 (160).
38. S. Mahalingam, S. Mohd Yunus, A. Manap, N. M. Afandi, R. A. Zainuddin, and N. F. Kadir, *Coatings* **9**, 2019 (719).
39. A. S. Praveen and A. Arjunan, *Applied Surface Science Advances* **7**, 2022 100191.
40. H. L. de Villiers Lovelock, P. W. Richter, J. M. Benson, and P. M. Young, *Journal of Thermal Spray Technology* **7**, 1998 (97–107).
41. I. Barin, *Thermochemical Data of Pure Substances*, (Wiley-Interscience, Germany, 2008).
42. N. Espallargas, Introduction to thermal spray coatings. in *Future Development of Thermal Spray Coatings*, ed. N. Espallargas (Amsterdam, Elsevier, 2015), p. 1.
43. T. S. Sidhu, A. Malik, S. Prakash, and R. D. Agrawal, *Journal of Thermal Spray Technology* **16**, 2007 (844).
44. R. Goyal, B. S. Sidhu, and V. Chawla, *Anti-Corrosion Methods and Materials* **65**, 2018 (217).
45. R. Kumar, V. K. Tewari, and S. Prakash, *Oxidation of Metals* **86**, 2016 (89).
46. V. Lépingle, G. Louis, D. Petelot, B. Lefebvre, and J. C. Vaillant, *MSF* **369–372**, 2001 (239).
47. S. Chandra-ambhorn and P. Saranyachot, *Journal of Materials Processing Technology* **268**, 2019 (18).
48. B. Hua, J. Pu, W. Gong, J. Zhang, F. Lu, and L. Jian, *Journal of Power Sources* **185**, 2008 (419).
49. J. Xiao, W. Zhang, C. Xiong, B. Chi, J. Pu, and L. Jian, *International Journal of Hydrogen Energy* **41**, 2016 (9611).
50. K. Nagata, *Solid State Ionics* **49**, 1991 (161).
51. F. Liu, J. E. Tang, T. Jonsson, et al., *Oxidation of Metals* **66**, 2006 (295).
52. M. Daroonparvar, M. A. Yajid, N. M. Yusof, et al., *Transactions of Nonferrous Metals Society of China* **23**, 2013 (1322).
53. L. Y. Ni, C. Liu, H. Huang, and C. G. Zhou, *Journal of Thermal Spray Technology* **20**, 2011 (1133).
54. E. J. Opila, D. L. Myers, N. S. Jacobson, et al., *ChemInform* **38**, 2007 (1971).
55. O. Kubaschewski and C. B. Alcock, *Metallurgical Thermochemistry*, (Pergamon, Oxford, 1979).
56. W. Huang, T. Huang, P. Song, et al., *Corrosion Science* **182**, 2021 109303.